Full-Wave Computation of Monostatic RCS Using Ray-Tracing and Adaptive Macro-Basis Functions

Carlos Delgado, Eliseo García, Lorena Lozano and Manuel Felipe Cátedra, *Life Fellow, IEEE*

***Abstract*—This paper presents a technique for the computation of the monostatic Radar Cross Section of complex objects based on a combination of Macro-Basis Functions and the Multilevel Fast Multipole Algorithm. An initial pool of excitation-independent Macro Basis Functions are first obtained, generating the corresponding reduced coupling matrix as well as the multipole data. For each excitation a ray-tracing processing is performed, extracting a number of critical points which are used to obtain a mask that allows to dynamically select the basis functions to be considered in the analysis. This strategy allows a noticeable reduction of the size of the problems with minimal CPU-time preprocessing overhead.**

***Index Terms*—Electromagnetic analysis, Moment methods, Numerical analysis, Ray Tracing.**

I. Introduction

THE prediction of the Radar Cross Section (RCS) of arbitrary targets constitutes a very important application of electromagnetic analysis methods, encompassing a broad range of operation fields that include, in addition to purely academic research, aircraft approach systems, vessel traffic service systems, collision-avoidance systems for terrestrial vehicles, meteorology, geology, health, law enforcement, military systems and others. The interest aroused by accurate RCS predictions has favored the emergence of efficient computation techniques, either in the form of general analysis approaches or restricted to the computation of the RCS for specific types of problems.

The estimation of the RCS for electrically large objects has been typically carried out using high-frequency techniques [1], [2]. The Geometric Theory of Diffraction (GTD) [3] is a cornerstone of this kind of approaches, incorporating diffraction effects to the existing Geometrical Optics (GO). The accuracy of this technique at caustics and light-shadowed boundaries, in turn, was improved by uniform theories, such as the Uniform Theory of Diffraction (UTD) [4]. The application of these approaches for arbitrary problems generally rely on detailed geometrical processing [5] to obtain the shadow boundaries and eclipse effects based on ray-tracing analyses [6] and their computational cost is associated to the number of geometric entities in the scenario rather than to the electrical size. However, when dealing with singular caustic curves or zones where many boundary layers overlap it may become necessary to resort to the computation of the surface field and integrate the currents in order to obtain the radiated field. The Physical Optics (PO) approach and the Physical Theory of Diffraction (PTD) [7] do not rely on the concept of rays, and calculate the current on each point of the surface as a function of the impinging incident field on that point. Fast quasi-analytical integration methods for the computation of the radiated fields can be seen in [8], [9].

In spite of the computational benefits carried by high-frequency techniques, some problems fall out of their scope in order to render reliable results or simply need a higher degree of accuracy. In these cases, and assuming limited computational resources, the next natural step is to combine asymptotic and rigorous methods in hybrid techniques, separating the geometrical domains in which each one is to be applied [10], [11].

The rise in computing power observed in the last years, specially with the increase of the number of cores and memory, together with an evolution of conventional full-wave techniques such as the Method of Moments (MoM) [12], has motivated the use of rigorous approaches to predict the RCS of scenarios that fell solely into the scope of asymptotic analysis some years ago. Domain decomposition techniques [13]–[15] reduce the computational cost by analyzing isolated parts of the scenario, followed by a data exchange process between domains. Full-wave analysis techniques based on enhancements of the Method of Moments have been developed in order to bypass the need to store the full coupling matrix, which is the main computational bottleneck of the MoM. Some of these approaches require to store only the near-field part of the matrix, avoiding the interactions between distant basis functions [16], [17], which are taken into account in the iterative resolution process using fast matrix-vector multiplications. Other techniques make use of high-level basis functions, often referred to as Macro Basis Functions (MBFs) [18]–[20], allowing an effective reduction of the number of unknowns typically of one order of magnitude. Different types of efficient techniques have been combined for an improved performance [21].

The rigorous analysis of monostatic RCS is an especially costly problem, because each observation direction requires the solution of the MoM equation system with a new excitation. Some existing approaches make use of a reduction of the number of problems when the set of excitations is rank-

This manuscript was submitted on XXX, 2019.

The work described in this paper has been supported in part by the Spanish Ministry of Economy and Competitiveness and European Union (Project Ref. TEC2017-89456-R), by the Junta de Comunidades de Castilla-La Mancha (Project Ref. SBPLY/17/180501/000433) and by the University of Alcalá (Project Ref. CCG2018/EXP-048).

Carlos Delgado, Lorena Lozano and Manuel Felipe Cátedra are with the Department of Computer Science, Universidad de Alcalá, Madrid 28801 Spain (e-mail: carlos.delgado@uah.es; lorena.lozano@uah.es; felipe.catedra@uah.es).

Eliseo García is with the Department of Automatics, Universidad de Alcalá, Madrid 28801 Spain (e-mail: eliseo.garcia@uah.es).

deficient [22]. Other approximations use the bistatic RCS in the close range of an excitation as an approximation of the monostatic solution [23], or apply an extrapolation based on the Asymptotic Waveform Extraction (AWE) technique [24], [25].

We propose here a novel approach for monostatic RCS computation based on a combination of the Multilevel Fast Multipole Algorithm (MLFMA) [16] with a MBF-derived approach in which the number of MBFs are dynamically selected from a primitive pre-computed set using a Ray-Tracing processing of the scenario under analysis. This allows a much more pronounced reduction of the number of unknowns while maintaining a high degree of accuracy.

This document is structured as follows: section II describes the ray-tracing considerations and the details of the proposed numerical technique. Some representative results are shown and discussed in section III. The conclusions and final remarks are presented in section IV.

II. Description of the analysis technique

This section contains the description of the technique proposed for the fast analysis of the monostatic RCS of complex scenarios. The total number of monostatic directions considered in the analysis is represented by N_m in this text. The application of a MBF-MLFMA based method requires, on one hand, the compartmentalization of the scenario into N_r cubical regions, whose size Δ_r is typically around $\lambda/4$ and, on the other hand, in terms of N_b blocks where the MBFs are defined, with a side length Δ_b of one or several wavelengths.

A. Ray-tracing processing

The technique proposed in this work makes use of the data retrieved by a ray-tracing analysis of the scenario for each monostatic direction. The authors have applied in past works ray-tracing data to speed up full-wave computations, reducing the effective size of the meshed scenario in [26] or considering the radiation pattern of antenna excitations to reduce the number of MBFs in [27]. In this work the ray-tracing analysis data is used to, instead of modifying the mesh as described in [26], reduce the size of the problem for each incidence direction by discarding macro-basis functions that do not have a significant contribution. The macro-basis functions are defined as aggregations of low-level conventional basis functions over blocks of the geometry, and therefore the mesh does not need to be altered. Note that the selection of MBFs for each block and excitation is dynamic in the sense that the threshold applied for their selection changes depending on the ray-tracing data provided. This is effectively equivalent to considering a different impedance matrix for each problem, where some macro-basis functions are discarded from the pre-computed pool if their relevance is deemed negligible. After obtaining the ray-tracing data, and with the purpose of developing an algorithm for the adaptive selection of MBFs independently for each monostatic direction, it is possible to get N_m sets of *critical points*, considering that a critical point represent the location of the interaction between a ray and the scenario (for example, reflection points, diffraction points or samples along the lines defining the trajectories of creeping waves). Fig. 1 shows an example containing an aircraft geometry and the ray-tracing analysis from a plane wave impinging from $\theta = 90°, \phi = 45°$. The bottom part of the Figure shows the scenario where the position of the critical points have been emphasized. Let us consider that there are $N_c^{(i)}$ critical points corresponding to the i-th incident direction, and the set of these points is denoted $C^{(i)}$, while the individual points are named $C_j^{(i)}$ with $j = 1 \cdots N_c^{(i)}$.

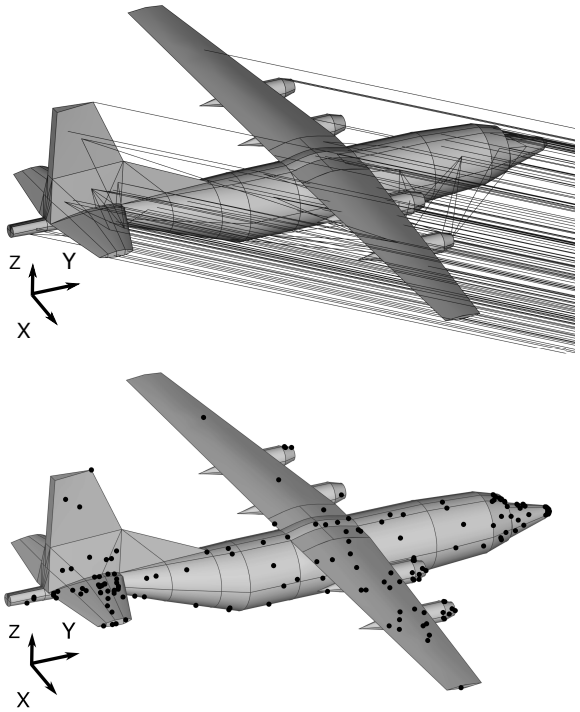

Fig. 1. Geometry, Ray-Tracing visualization (top) and illustration of the resulting critical points (bottom) for a commercial airplane. The excitation is a plane wave impinging from $\theta = 90^o, \phi = 45^o$.

1) Fast evaluation of shadowing tests: In order to identify efficiently the surfaces that are suitable candidates to intercept an incoming ray it is necessary to consider an ordering procedure based on their relative position. On this account, if there is an intersection between a ray $\vec{r}$ and a surface S_i all the surfaces situated behind S_i are eclipsed by S_i for that particular ray path. The facet-Angular Z-Buffer (AZB) algorithm [28] is a fast strategy to compute this relative ordering. The underlying methodology is based on the partition of the computational space in terms of angular elements called *anxels*. Each anxel represents a solid angle taking as the origin any of the vertices of the facet. For curved surfaces a preliminary facetization can be performed. The AZB of S_i is a matrix structure where the cells correspond to the anxels and each cell contains a list of the surfaces of the scenario located within the angular regions associated to it. The first element of the list corresponds to the closest surface. As a preliminary processing, the AZB structure of each facet of the scenario is obtained.

2) Computation of multiple effects: In addition to the calculation of the shadowing and intersection tests, the computation of effects of an arbitrary order on a realistic scenario can

be a formidable challenge applying a naïve implementation. Some techniques that allow to reduce this complexity are the methods based on images, allowing to reduce the order of the effect by substituting plane facets with their images, or those based on the minimization of the total length of the path for curved surfaces [5]. Shooting and bouncing rays (SBR) [6] techniques analyze all the rays shot in radial directions from the source. The rays which pass near the observation point are considered to contribute to the scattered field. The strategy followed in this work is based on a preliminary facetization of the scenario, followed by the identification of the illuminated facets by applying intersection tests using the AZB of the source of the ray. The critical points on that illuminated region are computed using the image of the source with respect to the tested facet. After determining the critical points due to the i-th effect the candidate facets for the (i+1)-th interaction are determined using the AZB of the previously illuminated facets in the angular region given by the outgoing ray, calculated using Snell's law [5]. More detailed information regarding this methodology can be seen in [28].

A special consideration needs to be given for the computation of the path followed by creeping waves [29]. In order to consider this effect it is necessary to identify first the silhouette points, which mark the interface between the visible and hidden parts of the object, and choose from these the entry and exit points. The creeping path is then computed taking into account the curvature of the object and the incident direction at the entry point. The path is defined by a set of sample points along the creeping contour.

B. Dynamic selection of MBFs and reduced matrix

In order to select dynamically the significant MBFs for each monostatic direction it is necessary to pre-compute a complete MBF pool, which is later used to generate a primitive reduced matrix. In the rest of this document the terms N_l and N_h make reference to the total number of low- and high-level basis functions, i.e., subdomain functions and MBFs, respectively, while a superscript, such as $N_l^{(i)}$ or $N_h^{(k)}$ indicates the basis functions contained in that specific block. The MBF pool is generated by isolating each block and orthogonalizing the currents induced by a set of external excitations. One approximation is based on the use of a sampling of the Plane Wave Spectrum (PWS) [19] as external sources. Considering angular separations of $\Delta\theta$ and $\Delta\phi$ degrees between plane waves, the total number of excitations is $P = \left[\frac{180^o}{\Delta\theta} \cdot \frac{360^o}{\Delta\phi}\right]$. Assuming that the current induced by the k-th plane wave on the i-th block is $[J_k^{(i)}]$, it is possible to include all the induced currents in a matrix $[J_{(PWS)}^{(i)}]$ and perform the Singular Value Decomposition:

$$\left[J_{PWS}^{(i)}\right] = \begin{pmatrix} \left\{\left[J_1^{(i)}\right]\right\}^T \\ \left\{\left[J_2^{(i)}\right]\right\}^T \\ \vdots \\ \left\{\left[J_P^{(i)}\right]\right\}^T \end{pmatrix} = \left[U^{(i)}\right]\left[\Sigma^{(i)}\right]\left[V^{(i)}\right]^* \quad (1)$$

where the columns of $\left[U^{(i)}\right]$ and $\left[V^{(i)}\right]$ are the left- and right-singular vectors which form orthonormal bases, and the diagonal part of $\left[\Sigma^{(i)}\right]$ contains the singular values $\sigma_1^{(i)}, \sigma_2^{(i)}, \cdots, \sigma_P^{(i)}$. Assuming that these values are arranged in increasing magnitude, a threshold T is used to truncate the number of columns of $[V^{(i)}]$ to be retained as the $N_h^{(i)}$ initial MBFs assigned to the i-th block as follows:

$$N_h^{(i)} = k \implies \frac{\sigma_1^{(i)}}{\sigma_k^{(i)}} \leq T \quad \text{and} \quad \frac{\sigma_1^{(i)}}{\sigma_{k+1}^{(i)}} > T \quad (2)$$

where typical values of 10^3 are generally found in the existing literature for the T parameter. As stated before, condition (2) indicates that the pool of MBFs of the i-th block is defined as the column vectors $\mathbf{v_k^{(i)}}$, with $k = 1 \cdots N_h^{(i)}$:

$$\left[V^{(i)}\right]_{N_l^{(i)} \times N_l^{(i)}} = \begin{pmatrix} \mathbf{v_1^{(i)}} & \mathbf{v_2^{(i)}} & \cdots & \mathbf{v_{N_h^{(i)}}^{(i)}} & \cdots & \mathbf{v_{N_l^{(i)}}^{(i)}} \end{pmatrix}. \quad (3)$$

It is necessary to follow this procedure for each block of the scenario, retaining the first $N_h^{(i)}$ values of $\left[\Sigma^{(i)}\right]$ in order to perform the fast dynamic assignation of MBFs from the existing pool as indicated below.

Note that the generation and storage of the MBF pool as previously described entails the need of additional computational resources compared to the conventional MoM-MLFMA. Considering that the $[J_k^{(i)}]$ currents in (1) are obtained using the PO approach the associated cost for their generation is $O(N_l^{(i)})$ and the storage of the matrix containing the currents increases with $O(P \cdot N_l^{(i)})$ where, as previously indicated, P and $N_l^{(i)}$ refer, respectively, to the total number of PWS excitations and the number of low-level basis functions contained in the i-th block. The computation of the SVD, in turn, increases as $O(N_l^{(i)} \cdot P^2 + P^3)$ as described in [30].

The MBFs can be described as aggregations of low-level basis functions using as weighting values the previously obtained coefficients:

$$J_j^{(i)}(\vec{r}) = \sum_{n=1}^{N_l^{(i)}} v_{j,n}^{(i)} T_n^{(i)}(\vec{r}) \quad (4)$$

where $v_{j,n}^{(i)}$ is the n-th element of $\mathbf{v_j^{(i)}}$, $J_j^{(i)}(\vec{r})$ stands for the j-th MBF on the i-th block and $T_n^{(i)}(\vec{r})$ is the n-th subdomain basis function on the same block. This expansion of the high-level basis functions allow to computed the reduced coupling matrix using the conventional low-level coupling coefficients. The coupling term between the m-th MBF of the i-th block and the n-th MBF of the j-th block can be expressed:

$$\left\langle L(J_n^{(j)}), J_m^{(i)} \right\rangle = \sum_{k=1}^{N_l^{(m)}} \sum_{p=1}^{N_l^{(n)}} v_{n,p}^{(j)} v_{m,k}^{(i)*} z_{k,p} \quad (5)$$

where the L operator computes the field radiated by the active MBF $J_n^{(j)}(\vec{r})$ over the passive MBF $J_m^{(i)}(\vec{r})$, and $z_{k,p}$ is the coupling term between conventional low-level basis functions. This expression allows to obtain the primitive reduced

matrix $[Z]$, that defines the system to be solved to obtain the current distribution corresponding to each excitation:

$$[Z][J_m] = [V_m], \text{ for m= 1..}N_m. \tag{6}$$

However, depending on the characteristics of the scenario and each incident direction, the solution of (6) can be equivalent to that of a further reduced system where the coupling matrix is tailored to the excitation:

$$[Z_m][J_m] = [V_m], \text{ for m= 1..}N_m \tag{7}$$

in this case $[Z_m]$, called effective reduced matrix, is a submatrix of $[Z]$ where a number of MBFs have been discarded taking into consideration the set of critical points for the m-th excitation, $C^{(m)}$. A procedure analogous to that described in (2) is followed in order to determine the number of effective MBFs to be retained, substituting T by a modified threshold value $T_m^{(i)}$, where m indicates the incident direction and i refers to the block, that can be determined as follows:

$$T_m^{(i)} = \begin{cases} T_{min} + \frac{\Delta_b^2 (T - T_{min})}{4 D_m^{(i)\,2}}, \text{if } D_m^{(i)} \geq \frac{\Delta_b}{2} \\ T, \text{if } D_m^{(i)} < \frac{\Delta_b}{2} \text{ or block-i contains caustics} \end{cases}, \tag{8}$$

where T_{min} is the minimum threshold value and $D_m^{(i)}$ is the distance between each block and the closest critical point for the m-th impinging plane wave:

$$D_m^{(i)} = \min_{j=1..N_c^{(m)}} (\| \vec{r}_b^{(i)} - \vec{r}_{C_j^{(m)}} \|) \tag{9}$$

where $\vec{r}_b^{(i)}$ makes reference to the position of the center of the i-th block and $\vec{r}_{C_j^{(m)}}$ is the position vector of the j-th critical point computed for the m-th excitation.

C. MLFMA application

The system matrix in (6) can be decomposed into its near and far field terms as follows:

$$\left([Z^{NF}] + [Z^{FF}] \right) [J_m] = [V_m], \text{ for m= 1..}N_m \tag{10}$$

where $[Z^{NF}]$ is the primitive near-field reduced matrix and can be computed using (5). This is a sparse matrix and will be later used to extract the effective reduced matrix for each monostatic direction. We propose to compute the far-field interactions between MBFs via the MLFMA, which allows to address larger problems and avoids the storage of $[Z^{FF}]$.

The partitioning of the scenario into first-level MLFMA regions considered makes use of the existing block structure ($\Delta_r = \Delta_b$). The clustering of these regions into higher groups is described by a hierarchical structure shaped as an octal tree. The interactions between MBFs located inside the same block, or in neighboring blocks, are computed using their coupling coefficients as described in (5), while those between distant MBFs are calculated computing the aggregation and disaggregation terms into first-level multipoles. This can be carried out considering the expansion of the MBFs into their low-level aggregations as seen in (4). The aggregation term for the j-th MBF of the m-th block at the first level can be thus expressed:

$$V_{mj}^{AGG(1)}(\hat{k}) = \sum_{k=1}^{N_l^{(m)}} \int_S v_{j,k}^{(m)} e^{-j\hat{k}\vec{r}_{jm}} (\bar{I} - \hat{k}\hat{k}) T_k^{(m)}(\vec{r'}) dS' \tag{11}$$

where $\vec{r}_{jm}$ is the position vector from each subdomain to the aggregation point at the center of the block. The disaggregation term for the i-th MBF located on the m'-th block at level 1 is analogously expressed as:

$$V_{m'i}^{DIS(1)}(\hat{k}) = \sum_{k=1}^{N_l^{(m')}} \int_S v_{i,k}^{(m')} e^{j\hat{k}\vec{r}_{im'}} (\bar{I} - \hat{k}\hat{k}) T_i^{(m')}(\vec{r'}) dS'. \tag{12}$$

Note that both the aggregation and disaggregation terms have only θ and ϕ components. The translator operator allows to express the multipole expansion that has been aggregated to $\vec{r_m}$ referred to a distant point at the same level $\vec{r'_m}$ and is given by:

$$\tau_{mm'}(\hat{k}, \vec{r}_{mm'}) = \frac{jk}{4\pi} \sum_{l=0}^{L} j^l (2l+1) h_l^{(1)}(kr_{mm'}) P_l(\vec{r}_{mm'} \cdot \hat{k}) \tag{13}$$

where $h_l^{(1)}(kr_{mm'})$ is a spherical Hankel function of the first kind and $P_l(\vec{r}_{mm'})$ is a Legendre polynomial. In order to apply a multilevel version of this strategy it is necessary to aggregate the multipoles belonging to the (l-1)-th level to their parent group at the l-th level:

$$V_{mj}^{AGG(l)}(\hat{k}) = V_{mj}^{AGG(l-1)}(\hat{k}) e^{-j\hat{k}\vec{r}_{m_{l-1}m_l}} \tag{14}$$

where $\vec{r}_{m_{l-1}}$ and $\vec{r}_{m_l}$ are the parent cube group centers of block m at levels $l-1$ and l, respectively. Likewise, the disaggregation from a parent cube at the (l+1)-th level down to its child cube at the l-th level can be written:

$$V_{m'i}^{DIS(l)}(\hat{k}) = V_{m'i}^{DIS(l+1)}(\hat{k}) e^{j\hat{k}\vec{r}_{m_{l+1}m_l}}. \tag{15}$$

III. Numerical Results

This section contains a selection of examples where the efficiency and performance of the previously described approach have been assessed. The CPU-time values shown have been obtained using a parallel implementation of the analysis methods running on 2 Intel Xeon processors with a base clock speed of 2.9 GHz, 16 physical cores and 256 GB of RAM. The iterative solver used in the simulations has been the Biconjugate Gradient Stabilized (BiCGStab) [31] with an maximum error of 10^{-3}. The proposed approach has been named "Dynamic RT-MBF" in the plots showing the monostatic RCS results. The geometries have been meshed taking into account the conventional sampling rate of $\lambda/10$.

A. PEC Ogive

The first test case considered in this section is a metallic ogive. This is a classic RCS test case for measurement and simulation, and the specific model used is described in [32]. This ogive has a total length of 10 inches (or 25.4 cm) and a half-angle of 22.62°. The geometry has been generated following the analytical expressions:

$$\begin{aligned} &\text{for } -5 \leq t \leq 5 \text{ and } -\pi \leq \phi \leq \pi : \\ &\quad x = t \\ &\quad f(x) = \sqrt{1 - \left(\frac{x}{5} \cdot \sin(22.62^\circ)\right)^2} - cos(22.62^\circ) \\ &\quad y = \frac{f(x) \cdot \cos(\phi)}{1 - \cos(22.62^\circ)} \\ &\quad z = \frac{f(x) \cdot \cos(\phi)}{1 - \sin(22.62^\circ)} \end{aligned} \tag{16}$$

where the length units, related to the t parameter, are expressed in inches. The resulting object is illustrated in Fig. 2.

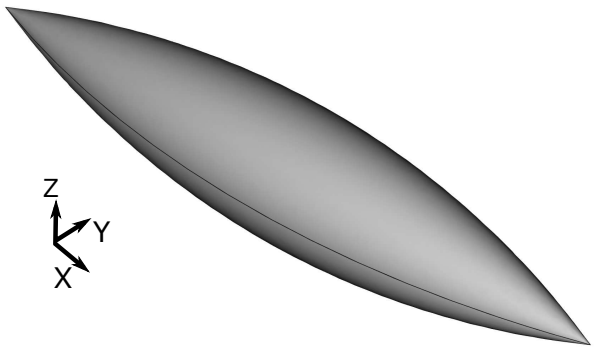

Fig. 2. Geometrical model of the PEC ogive.

The monostatic RCS has been calculated for this geometry at a frequency of 100 GHz, considering the Combined Field Integral Equation (CFIE) formulation and the angular observation directions ranging in azimuth from $\phi = 0^\circ$ to $\phi = 180^\circ$ for $\theta = 90^\circ$. Both polarizations have been considered using the MoM-MLFMA, MBF-MLFMA and the proposed approach. The results for the $\theta - \theta$ and $\phi - \phi$ polarizations are shown in Figs. 3 and 4, respectively. The CPU-time required by the analysis methods considered for each incident polarization is shown in Table I, differentiating the pre-processing and the solution stages. The total number of basis functions has been 616,952 with the MoM-MLFMA, 189,039 MBFs with the MBF-MLFMA and an average of 114,090 MBFs per monostatic direction considering the proposed approach.

The data contained in Table I shows the extra pre-processing time required by MBF-based techniques in order to generate the high-level basis functions compared to the conventional MoM-MLFMA approach. Note that the proposed approach does not include any additional time over the conventional MBF technique due to the generation of the MBF pool, because all the MBFs contained in the pool are required by the conventional approach for each individual excitation.

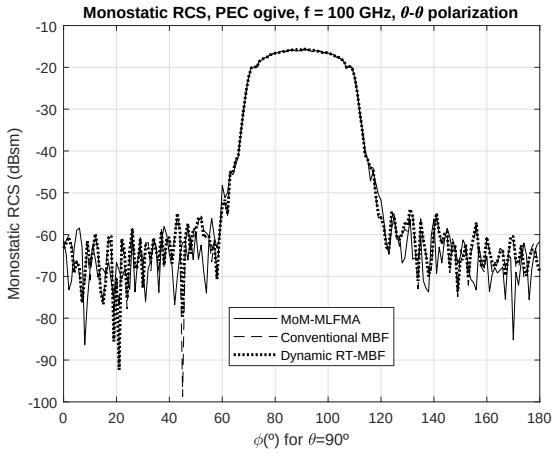

Fig. 3. Monostatic RCS results for the metallic ogive comparing MoM-MLFMA, a conventional MBF technique and the proposed approach ($\theta - \theta$ polarization).

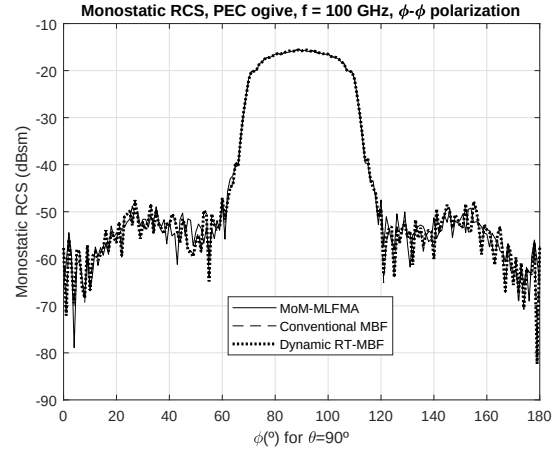

Fig. 4. Monostatic RCS results for the metallic ogive comparing MoM-MLFMA, a conventional MBF technique and the proposed approach ($\phi - \phi$ polarization).

TABLE I
CPU-TIME REQUIRED FOR THE PEC OGIVE TEST CASE (SECONDS).

Analysis Method	Polarization	Pre-Processing	Solution
MoM-MLFMA	θ	581	15,636
MBF-MLFMA	θ	1,930	5,469
Proposed Technique	θ	1,930	3,721
MoM-MLFMA	ϕ	581	15,272
MBF-MLFMA	ϕ	1,930	5,718
Proposed Technique	ϕ	1,930	3,959

B. Airliner

This test case makes use of the Perfect Electric Conductor (PEC) geometrical model of the airliner shown in Fig. 1, previously used to illustrate the technique proposed in this work. This scenario includes 257 Non-Uniform Rational B-Spline (NURBS) surfaces. The monostatic RCS has been obtained at 1 GHz considering a θ polarized incident field for the angular cut given by $\theta = 90^o$ and ϕ ranging from 0^o to 180^o in 1^o

steps. This is a closed geometry, which allows the analysis using the CFIE for a faster convergence. The results obtained using the proposed approach have been compared to those provided by the application of conventional MoM-MLFMA and MBF-MLFMA techniques. The accuracy is remarkably good in this case, both for the co-polar and cross-polar components, shown respectively in Figs. 5 and 6. The total number of low-level unknowns has been 1,784,241 and is reduced to 556,234 MBFs with the conventional MBF-MLFMA method, while the proposed technique has produced an average of 389,223 MBFs in the angular observation range. The total CPU-time has been broken down into the pre-processing time, including only the MLFMA data retrieval, coupling matrix assembly and, if applicable, the MBF generation, and the solution time, and is indicated in Table II, corroborating the expected efficiency improvement of the proposed approach.

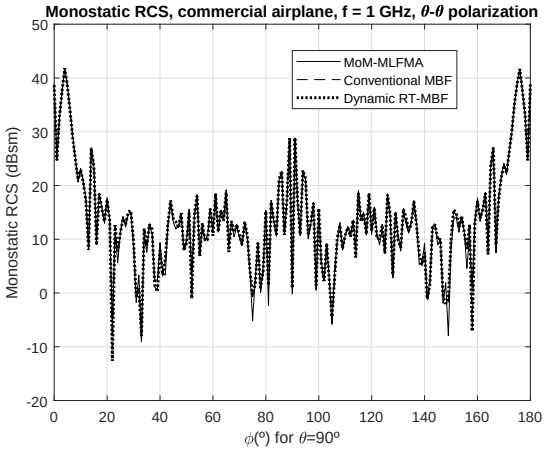

Fig. 5. Monostatic RCS results for the commercial aircraft scenario comparing MoM-MLFMA, a conventional MBF technique and the proposed approach ($\theta - \theta$ polarization).

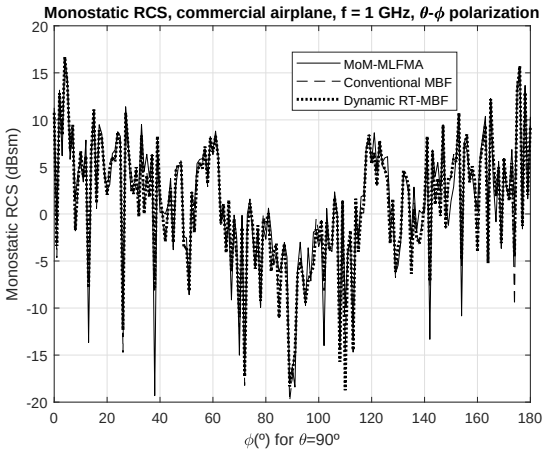

Fig. 6. Monostatic RCS results for the commercial aircraft scenario comparing MoM-MLFMA, a conventional MBF technique and the proposed approach ($\theta - \phi$ polarization).

TABLE II
CPU-TIME REQUIRED FOR THE AIRLINER TEST CASE (SECONDS).

Analysis Method	Pre-Processing	Solution
MoM-MLFMA	1,698	117,769
MBF-MLFMA	6,790	45,940
Proposed Technique	6,790	28,982

C. Small jet airplane

This test case involves a PEC jet airplane modeled using 321 NURBS patches and depicted in Fig. 7. It is an open geometry, precluding the use of CFIE, and therefore the monostatic RCS has been computed considering the Electric Field Integral Equation (EFIE), which generally presents slower convergence properties. The monostatic RCS analysis has been performed considering a θ polarized excitation and the observation angular range given by $\phi = 180^o$ and $\theta = 0^o$ to $\theta = 90^o$ with a separation of 3^o between angular samples. The frequency considered has been 1 GHz, rendering 333,150 low-level unknowns, 110,240 MBFs when applying the conventional MBF-MLFMA technique and and average of 74,513 MBFs using the proposed method. The CPU-time required by the simulations is shown in Table III.

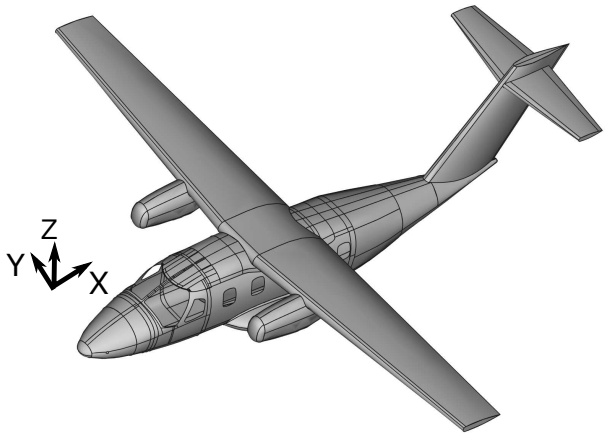

Fig. 7. Geometrical model of a small jet airplane.

TABLE III
CPU-TIME REQUIRED FOR THE SMALL JET AIRPLANE TEST CASE (SECONDS).

Analysis Method	Pre-Processing	Solution
MoM-MLFMA	261	221,618
MBF-MLFMA	1,639	148,476
Proposed Technique	1,639	103,700

IV. CONCLUSION

A numerical full-wave approach for the computation of the monostatic RCS of complex scenarios has been presented in this work. It makes use of a pre-computed near-field coupling matrix using a primitive pool of MBFs as well as

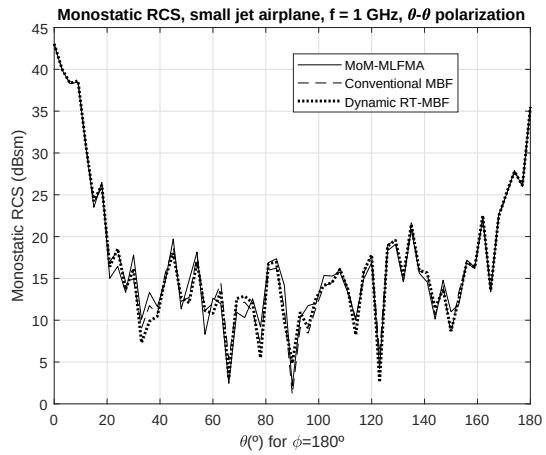

Fig. 8. Monostatic RCS results for the small jet airplane comparing MoM-MLFMA, a conventional MBF technique and the proposed approach ($\theta - \theta$ polarization).

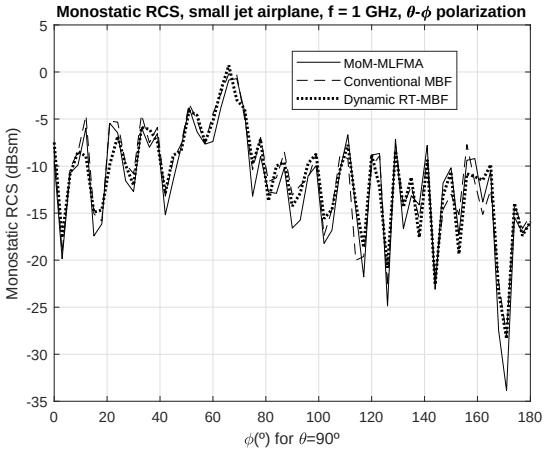

Fig. 9. Monostatic RCS results for the small jet airplane comparing MoM-MLFMA, a conventional MBF technique and the proposed approach ($\theta - \phi$ polarization).

a combination with the MLFMA. For each incident plane wave a ray-tracing process is carried out, identifying the the critical points that are subsequently used to create a mask that serves to reduce the effective size of the primitive coupling matrix, resulting in shortened CPU-time requirements. Since the coupling data is obtained in a pre-processing stage there is not any additional run-time overhead over conventional MBF-based approaches. Some representative test cases show very good accuracy in the results and improved efficiency.

REFERENCES

[1] D.P. Bouche, F.A. Molinet, R. Mittra, "Asymptotic and hybrid techniques for electromagnetic scattering", *Proc. IEEE*, vol. 81, no. 12, pp. 1658-1684, Dec. 1993.

[2] E. F. Knott, "A Progression of High-Frequency RCS Prediction Techniques", *Proceedings of the IEEE*, vol. 73, no. 2, pp. 252-264, Feb. 1985.

[3] J. B. Keller, "Geometrical Theory of Diffraction," *J. Opt. Soc. Amer.*, vol. 52, pp. 116-130, 1962.

[4] R. C. Kouyoumjian, P. H. Pathak, "A Geometrical Theory of Diffraction for an Edge in a Perfectly Conducting Surface," *Proc. IEEE.*, vol. 62, pp. 1448-1461, Nov. 1974.

[5] L. Lozano, M. J. Algar, E. García, I. González, F. Cátedra, "Efficient Combination of Acceleration Techniques Applied to High-Frequency Methods for Solving Radiation and Scattering Problems," *Computer Physics Communications*, vol. 221, pp. 28-41, Dec. 2017.

[6] F. Weinmann, "Ray Tracing with PO/PTD for RCS Modeling of Large Complex Objects", *IEEE Trans. Antennas Propagat.*. vo1. 54, no. 6, pp. 1797-1806,June 2006.

[7] P. Ya. Ufimtsev, "Elementary Edge Waves and the Physical Theory of Diffraction," *Electromagnetics*, vol. 11, pp. 125-160, 1991.

[8] M. F. Cátedra, C. Delgado, S. Luceri, F. Sáez de Adana, "Efficient procedure for computing fields created by current modes", *Electronics Letters*, vol. 39, pp. 763-764, May 2003.

[9] M. F. Cátedra, C. Delgado, S. Luceri, O. G. Blanco, F. Sáez de Adana, "Physical optics analysis of multiple interactions in large scatters using current modes", *IEEE Trans. Antennas Propagat.*, vol. 54, no. 3, pp. 985-994, March 2006.

[10] L.N.Medgyesi-Mitschang and Dau-Sing Wang, "Hybrid methods in computational electromagnetics: a review", *Computer Physics Communications*, vol. 68, no. 1-3, pp. 76-94, Nov. 1991.

[11] U. Jakobus, F. M. Landstorfer, "Improved PO-MM hybrid formulation for scattering from three-dimensional perfectly conducting bodies of arbitrary shape", *IEEE Trans. Antennas Propagat.*, vol. 43, no. 2, pp. 162-169, Feb. 1995.

[12] R. F. Harrington, *"Field Computation by Moment Methods"*, New York, McMillan, 1968.

[13] I. Gonzalez, A. Tayebi, J. Gomez, C. Delgado, M. F. Cátedra, "Fast Analysis of a Dual-Band Reflectarray Using Two Different Numerical Approaches Based on the Moment Method", *IEEE Trans. Antennas Propagat.*, vol. 61, no. 4, pp. 2333-2336, April 2013.

[14] K. Zhao, V. Rawat, J.-F. Lee, "A domain decomposition method for electromagnetic radiation and scattering analysis of multi-target problems", *IEEE Trans. Antennas Propagat.*, vol. 56, pp. 2211-2221, Aug. 2008.

[15] C. Delgado, E. García, M. F. Cátedra, "Ray-Tracing Based Dual Domain Analysis Technique Using the Method of Moments and the Multilevel Fast Multipole Algorithm", *IEEE Trans. Antennas Propagat.*, vol. 67, no. 12, pp. 7496–7504, Dec. 2019.

[16] J. M. Song, W. C. Chew, "Multilevel Fast Multipole Algorithm for Solving Combined Field Integral Equations of Electromagnetic Scattering", *Microwave and Optical Technology Letters*, vol. 10, no. 2, pp. 14-19, Sept. 1995.

[17] J. M. Tamayo, A. Heldring, J. M. Rius, "Multilevel Adaptive Cross Approximation (MLACA)", *IEEE Trans. Antennas Propagat.*, vol. 59, no. 12, pp. 4600-4608, Dec. 2011.

[18] V. V. S. Prakash and R. Mittra, "Characteristic Basis Function Method: A New Technique for Efficient Solution of Method of Moments Matrix Equation", *Micr. Opt. Technol. Letters*, vol. 36, no. 2, pp. 95-100, Jan. 2003.

[19] C. Delgado, R. Mittra, M. F. Cátedra, "Accurate Representation of the Edge Behavior of Current when Using PO-derived Characteristic Basis Functions", *IEEE Antennas and Wireless Propagation Letters*, vol. 7, no. 5, pp. 43-45, March 2008.

[20] C. Delgado, M. F. Cátedra, "Efficient Generation of Macro Basis Functions for Radiation Problems Using Ray-Tracing Derived Dynamic Thresholds", *IEEE Trans. Antennas Propagat.*, vol. 66, no. 6, pp. 3231-3236, June 2018.

[21] E. Garcia, C. Delgado, I. González, M. F. Cátedra, "An Iterative Solution for Electrically Large Problems Combining the Characteristic Basis Function Method and the Multilevel Fast Multipole Algorithm", *IEEE Trans. Antennas Propagat.*, vol. 56, no. 8, pp. 2363-2371, Aug. 2008.

[22] Z.-Q. Lu, X. An, "Fast monostatic radar cross-section computation for perfectly electric conducting targets using low-rank compression and adaptive integral method", *IEEE Trans. Antennas Propagat.*, vol. 52, no. 2, pp. 605-607, Feb. 2004.

[23] M. J. Schuh, A. C. Woo, M. P. Simon, "The Monostatic/Bistatic Approximation", *Electromagnetics*, vol. 36, no. 4, pp. 76-78, Aug. 2004.

[24] Y. E. Erdemli, J. Gong, C. J. Reddy, J. L. Volakis, "Fast RCS pattern fill using AWE technique", *IEEE Trans. Antennas Propagat.*, vol. 46, pp. 1752-1753, Nov. 1998.

[25] X. C. Wei, Y. J. Zhang, E. P. Li, "The hybridization of fast multipole method with asymptotic waveform evaluation for the fast monostatic RCS computation", *IET Microw. Antennas Propag.*, vol. 8, no. 1, pp. 46-51, Jan. 2014.

[26] C. Delgado, M. F. Cátedra, "Combination of Ray-Tracing and the Method of Moments for Electromagnetic Radiation Analysis using Reduced Meshes", *Journal of Computational Physics*, vol. 361, pp. 412-423, May 2018.

[27] C. Delgado, M. F. Cátedra, "Dynamic Threshold Selection Based on Radiation Pattern Characteristics for the Generation of Macro Basis Functions", *IEEE Antennas and Wireless Propagation Letters*, vol. 17, no. 10, pp. 1812-1816, Oct. 2018.

[28] M. F. Cátedra, L. Lozano, I. González, E. García, M. J. Algar, "Efficient Techniques for Accelerating the Ray-Tracing for Computing the Multiple Bounces Scattering of Complex Bodies Modeled by Flat Facets", *Applied Computational Electromagnetics Society Journal*, vol. 25 , no. 5 , pp. 395-409, May 2010.

[29] L. Lozano, F. Sáez de Adana, M. F. Cátedra, "Contribution of the Illuminated and Shadowed Areas in the Radiation Pattern of On-Board Antennas", in Proc. 5th International Conference on Electrical Engineering, Computing Science and Automatic Control, 12-14 Nov. 2008, pp. 248-251, Mexico City, Mexico.

[30] G. H. Golub and C. van Loan, *"Matrix Computations"*. Baltimore, MD:The Johns Hopkins Univ. Press, 1989.

[31] G. L. G. Sleijpen and D. R. Fokkema, "Bi-CGSTAB(l) for Linear Equations Involving Unsymmetric Matrices with Complex Spectrum", *Elec. Trans. Numer. Anal.*, vol. 1, pp. 11-32, 1993.

[32] C. Woo, H. T. G. Wang, M. J. Schuh, M. L. Sanders, "EM Programmer's Notebook-Benchmark Radar Targets for the Validation of Computational Electromagnetics Programs", *IEEE Antennas and Propagation Magazine*, vol. 35, no. 1, pp. 84-89, Feb. 1993.